Article

Synthesis, Characterization, and Synergic Photocatalytic Activity of Amorphous TiO₂/Chitosan Carbon Microspheres

Liziê D. T. Prola,[a] Larissa Bach-Toledo,[a] Juliana Schultz,[a] Antonio S. Mangrich [a,b] and Patricio G. Peralta-Zamora [*,a]

aDepartamento de Química, Universidade Federal do Paraná, CP 19032, 81531-980 Curitiba-PR, Brazil

bInstituto Nacional de Ciência e Tecnologia - Energia e Meio Ambiente (INCT E&A), 40170-155 Salvador-BA, Brazil

In this work, we report the synthesis and characterization of new amorphous graphene-like TiO₂/chitosan carbon microspheres and its performance as photocatalyst. Four different carbon chitosan microspheres materials were obtained based on the distinctive procedure to incorporate TiO₂ and TiOSO₄ to chitosan structure by pyrolysis at 600 °C. Detailed characterizations were carried out using many different techniques, as thermogravimetric analysis/differential scanning calorimetry (TGA/DSC), scanning electron miscroscopy/energy dispersive X-ray spectroscopy (SEM/EDS), Fourier transform infrared spectroscopy (FTIR), X-ray photoelectron spectroscopy (XPS), X-ray diffraction (XRD), N₂ adsorption-desorption, and the obtained materials show an amorphous and a graphene-like structure, which improve the photocatalytic activity. The synthesized materials promoted a fast degradation of three micropollutants under UV-A radiation and, in all cases the degradation rate was approximately 98% at 30 min of reaction, being superior to the P-25 TiO₂ efficiency. Due to the amorphous graphene-like structure, all the materials present low adsorption capacity, the high photocatalytic efficiency can be attributed to the material structure that promotes the effective charge separation which reduces the recombination electron/hole, enhancing the photocatalytic efficiency.

Keywords: chitosan, heterogeneous photocatalysis, amorphous graphene-like carbon, carbonization, pharmaceutical degradation

Introduction

Detection of pharmaceutical compounds, personal care products, pesticides, and a variety of endocrine-disrupting compounds in aquatic ecosystems, even at low concentrations, has become a worldwide concern due to the potential environmental impacts.[1-3] Domestic sewage is a major source of organic compounds that can contaminate the aquatic environment, even after treatment by conventional wastewater treatment plants (WWTPs). For example, many antibiotics can be excreted by humans in their active form and are partially removed by conventional sewage treatment systems.[4] Consequently, antibiotics occurrence in the aquatic environment can trigger bacterial resistance.[4,5]

Most conventional WWTPs are not designed to eliminate these organic compounds at low concentrations (ng L⁻¹ or μg L⁻¹). Therefore, there is a necessity for additional tertiary treatments[6,7] that enable the wastewater to be reused.[8] Various alternative processes have been studied for this purpose, including treatments based on the use of membranes,[9] specific microorganisms,[10] and advanced oxidation processes (AOPs).[11]

Among the different AOPs, heterogeneous photocatalysis is an attractive process that has shown high degradation efficiency of several organic pollutants present in aqueous media. The fundamentals of heterogeneous photocatalysis have been very well documented,[12] including the high photocatalytic activity of TiO₂.[13] Due to its useful features, considerable efforts have been focusing on the synthesis of immobilized forms of TiO₂, mainly to facilitate its recovery and reuse.[13]

A variety of techniques have been proposed for the immobilization of TiO₂ on support matrices including borosilicate glass,[14] cellulose,[15] silica,[16] zeolites,[17] polymers,[18] and carbonaceous materials.[19] Composites

*e-mail: zamora@ufpr.br

containing TiO$_2$ and carbonaceous materials, such as activated carbon, carbon nanotubes,[20] and graphene,[21] have been widely used in photocatalytic processes, mainly due to their well established synergistic effects.[19] The high adsorption capacity of some carbonaceous materials, allied to a high charge carrier mobility and low electron-hole pair recombination, allows the efficient degradation of many environmental pollutants.[19,22]

In the last 30 years, studies[22] have explored the association between photocatalysts and sorbents, due to the favorable effect of the initial adsorption of substrates on the photocatalyst surface. Particular interest has focused on the use of activated carbon (AC)[23] as a high-surface-area amorphous material employed as a support for TiO$_2$, improving not only the stability and durability but also its optical activity in the visible region.[14,24] Substantial improvements in photocatalytic efficiency have been reported due to the use of this association. For example, Baek *et al.*[25] described several advantages associated with the use of spherical activated carbon (SAC) prepared from ion-exchange resin, including better fluidity, greater mechanical strength, and lower resistance to the diffusion of liquids.

Polymeric materials are also widely used as photocatalyst supports, in order to assist in the recovery and reuse of catalysts. Chitosan (CS), a semi-synthetic polymer produced by deacetylation of chitin, has a unique structure, useful functionalities, and a wide range of applications[26] including the adsorption of heavy metals and dyes from aqueous solutions.[27] Zawadzki and Kaczmarek[28] studied the thermal decomposition of chitosan and its potential for the generation of activated carbon. Important changes in the chemical structure of chitosan were observed at temperatures from 50 to 600 °C, including the opening of pyranose rings and the simultaneous formation of polyaromatic carbonaceous residues.

Despite the existence of many materials produced from chitosan, including activated carbon, there are few reports of its use as a precursor of SAC, in order to act as support of photocatalysts. Hamden *et al.*[29] used the chitosan as a template for the generation of TiO$_2$ nanoparticles. The material was prepared via a non-hydrolytic sol-gel approach in *tert*-butanol for aniline photocatalytic degradation. According to the results, CS-TiO$_2$ samples heat-treated at 50 and 300 °C reached aniline degradation of 5 and 33%, respectively, after 9 h visible light irradiation. Zhu *et al.*[30] synthesized CdS nanocrystals deposited on TiO$_2$/crosslinked chitosan composite (CSC) dried at 60 °C under the atmospheric condition to discoloration of methyl orange in aqueous solution. The photocatalytic dye discoloration reached 99.1% by CdS/TiO$_2$/CSC after simulated solar light irradiation for 210 min.

Therefore, the present work describes, for the first time, the use of chitosan as a natural template for the immobilization of TiO$_2$ on spherical amorphous graphene-like carbon material, employed as a semiconductor to be used in heterogeneous photocatalysis. The evaluation of the photocatalytic activity of this composite was preliminarily carried out on an aqueous solution of sulfamethoxazole, an antibiotic that habitually occurs in drinking water around the world, being considered as a relevant emerging pollutant.[31] Afterward, the study was extended to chloramphenicol and hydrochlorothiazide, drugs that are also often found in natural waters.

Experimental

Chemicals

Sulfamethoxazole (SMX), titanium tetra-isopropoxide (TTIP), and chloramphenicol (CRP) (purities > 97%) were purchased from Sigma-Aldrich (Steinheim, Germany). Hydrochlorothiazide (HCT) was supplied by Farmanguinhos Fio Cruz (Rio de Janeiro, Brazil). Polymar (Fortaleza, Brazil) kindly provided chitosan (CS) (degree of deacetylation ≥ 95%). P-25 TiO$_2$ (50 m^2 g^{-1}; 85-70% anatase + 15-30% rutile; mean particle diameter of 30 nm) was kindly provided by Degussa (Frankfurt, Germany). Isopropyl alcohol, acetic acid, and glutaraldehyde (50% m/v) were purchased from Biotec (São Paulo, Brazil). All chemicals were used without further purification. The water employed in all the procedures was deionized followed by purification using a Milli-Q system (Millipore, Bedford, MA, USA).

Synthesis of TiO$_2$/carbon microspheres

The TiO$_2$-modified carbon microspheres were prepared from a solution of CS (4.0 g) in acetic acid (HAc, 80 mL, 5% v/v), using two different strategies (see Figure 1). In the first procedure, chitosan beads were formed by dropwise addition of the CS solution to a solution of sodium hydroxide (2 mol L^{-1}) containing either TiO$_2$ (2 g) or TiOSO$_4$ (2 g), resulting in the formation of microspheres (denoted CS/Ti/C-1 and CS/TiS/C-1, respectively). The microspheres were then washed until reaching pH 7, followed by immersion in a known volume of an aqueous solution of glutaraldehyde (1% v/v) during 17 h. Finally, at the end of this period, the microspheres were washed with deionized water.

In the second procedure, chitosan beads were prepared and crosslinked as described above, followed by leaving in contact with TiO$_2$ (0.4 g) in ethanol or TiOSO$_4$ (0.8 g)
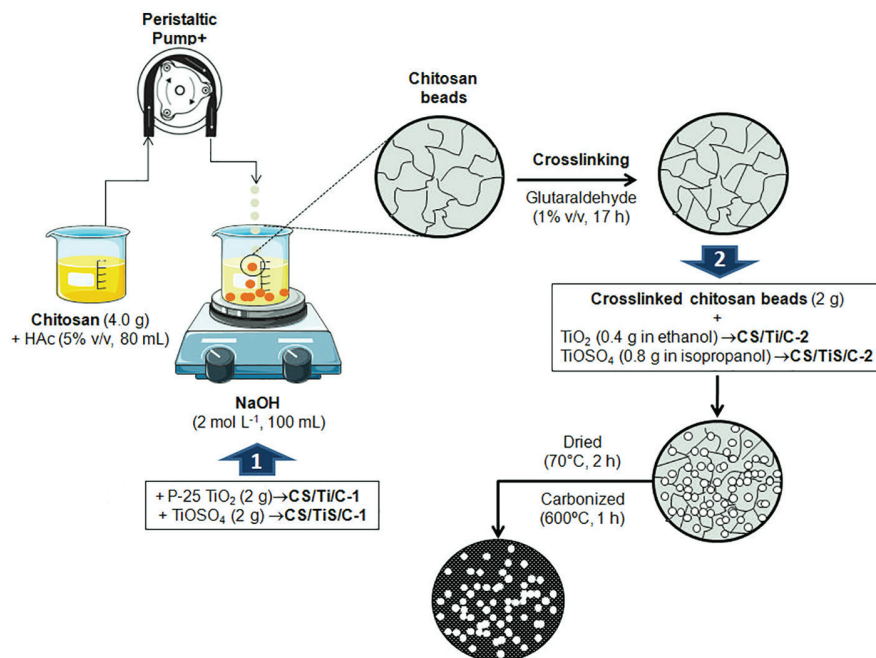
Figure 1. Synthesis of TiO$_2$/carbon microspheres scheme.

in isopropanol, for 24 h, resulting in the formation of microspheres denoted CS/Ti/C-2 and CS/TiS/C-2, respectively.

In both procedures, the composite microspheres were dried at 70 °C for 2 h and were subsequently carbonized at 600 °C for 1 h, in an oxygen-deficient atmosphere, using a heating rate of 10 °C min⁻¹ (FT-HI/40, EDG Equipamentos, Brazil) (Figure 1).

Characterization of the TiO$_2$/carbon microspheres

The morphology of the materials was characterized by scanning electron microscopy (SEM), using an FEI Quanta 450 FEG scanning electron microscope equipped with an energy dispersive X-ray analyzer (EDS) for elemental mapping. The crystal structures of the materials were characterized by X-ray diffraction (XRD), using a Shimadzu XRD-7000 X-ray diffractometer operating at 40 kV and 20 mA. The diffractograms were obtained in the 2θ range from 20 to 80°, with Cu Kα radiation at a wavelength of 1.5418 Å. Raman spectra were acquired with a WITec Alpha 300R confocal microscope, using a 532 nm laser excitation line. The spectra were obtained in the range from 50 to 1200 cm⁻¹, at a resolution of 3 cm⁻¹.

Functional groups were characterized by Fourier transform infrared spectroscopy (FTIR) in the region 400-4000 cm⁻¹, using a Bomem Michelson MB100 spectrometer. The analyses were performed using the KBr pressed disk technique, with spectra recorded at a resolution of 4 cm⁻¹ and accumulating 32 scans. X-ray photoelectron

spectroscopy (XPS) analyses employed a VG Microtech ESCA3000 instrument, with Al/Mg Kα radiation, base pressure of 10-9 mbar, and overall energy resolution of 0.8 eV. All the binding energies were calibrated using the C 1s binding energy value (284.6 eV) and the peaks were well fitted with symmetric Gaussian-Lorentzian functions. Textural characterization was performed with a Quantachrome Nova 2000e equipment.

The surface area was determined by the Brunauer-Emmett-Teller (BET) method, while the pore size distribution was obtained by the Barrett-Joyner-Halenda (BJH) method. To perform the thermogravimetric analysis (TGA) a NETZSCH STA 449 F3 Jupiter analyzer was employed, with heating from 25 to 1000 °C, at a rate of 10 °C min⁻¹, in an atmosphere of synthetic air at a flow rate of 50 mL min⁻¹. The bandgap energy was measured in a Shimadzu UV-240 PC, by UV-Vis diffuse reflectance spectroscopy.

Analysis of photocatalytic performance

The photocatalytic activity of the composites was evaluated by measuring the degradation of individual compounds in aqueous solution, under UV-A radiation. The experiments were conducted at 25 ± 2 °C in a 250 mL batch photochemical reactor equipped with a water-cooling system and a magnetic stirrer. Each experiment consisted in 200 mL of SMX (5 mg L⁻¹) at pH 4, previously studied in our research group,[32] and the photocatalysts: chitosan (100 mg), P-25 TiO$_2$ (20 mg), or the synthesized materials

(CS/Ti/C-1, CS/Ti/C-2, CS/TiS/C-1, or CS/TiS/C-2, in amounts equivalent to 20 mg of TiO$_2$). The mixtures were stirred for 5 min in the dark, in order to achieve adsorption-desorption equilibrium. The suspensions were then irradiated with UV-A for 60 min using a 125 W high-pressure mercury vapor lamp (without the original glass bulb), which was covered with a Pyrex bulb and inserted into the solution. To evaluate the degradation, spectrophotometric and liquid chromatographic analyses were performed. Thus, aliquots (3 mL) were collected at regular intervals and filtered through a 0.45 μm Millex-HA filter (Millipore). It is important to emphasize that microspheres were easily removed from the solution, since they usually float, however, it was essential to filter the solution to the chromatographic analysis.

Analytical conditions

Separation and determination of SMX, CRP, and HCT were performed by high-performance liquid chromatography with diode array detection (HPLC-DAD), using an Agilent 1260 system equipped with an autosampler and a quaternary pump. The substrates were determined separately using a C18 column (Microsorb-MV 100-5, 250 × 4.6 mm, 5 μm particle size) coupled to a guard column (12.5 × 4.6 mm) packed with the same stationary phase. The elution was performed at 30 ± 0.8 °C, using a gradient of ultrapure water and acetonitrile at flow rates of 1.0 mL min^{-1} for SMX and 0.6 mL min^{-1} for CRP and HCT. The DAD wavelength was set at 280 nm for CRP and 270 nm for SMX and HCT.

Results and Discussion

Carbonization of reticulated chitosan beads

The thermal behavior of the reticulated chitosan beads was evaluated by thermogravimetry/differential scanning calorimetry (TG/DSC) in an oxygen-limiting atmosphere, which revealed essentially three thermal events (Figure 2). The first (up to 235 °C, with weight loss of approximately 14%) was related to the removal of physically adsorbed water (below 100 °C), strongly hydrogen-bonded water (below 140 °C), and volatile compounds such as acetic acid from the solvent.[33] The second event (in the range between 235 and 535 °C) corresponded to greater changes in the chitosan chemical structure, including deacetylation and depolymerization. According to characterization studies carried out by FTIR, temperatures between 200 and 250 °C cause drastic changes in the chemical structure of chitosan, including depolymerization and reactions involving the

opening of pyranose rings.[34] At temperatures around 300 °C, the structure of the chitosan collapses, with the formation of aliphatic structures, while at higher temperatures (400 to 500 °C) there is an intense decomposition of the aliphatic structures and the concomitant appearance of aromatic structures.[34] The third thermal event, represented by an exothermic peak centered at 568 °C, corresponds to the pyrolysis process, which leads to the formation of a polyaromatic network with a structure equivalent to the activated carbon.[28] Due to this thermal behavior, the carbon microspheres were produced by carbonization at 600 °C in an oxygen-limiting atmosphere.
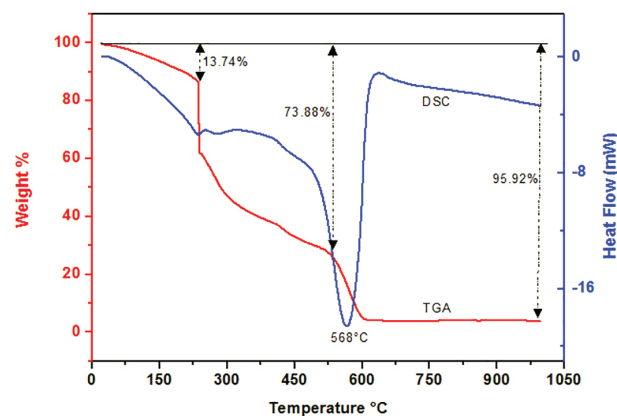

Figure 2. TGA-DSC analysis of crosslinked chitosan.

Characterization of the materials

The surface morphologies of the composite microspheres were investigated by SEM/EDS analysis. The SEM images of all the materials revealed spherical-like shapes with sizes between 500 and 800 μm (Figure 3). The EDS micrographs showed that the immobilization of TiO$_2$ (CS/Ti/C-2) and TiOSO$_4$ (CS/TiS/C-2) on the crosslinked chitosan beads resulted in cracked surfaces that were homogeneously coated with Ti (Figures 3a and 3b). The material prepared from TiOSO$_4$ presented a mixture of carbon and sulfur within the cracks, due to incomplete transformation of the titanyl sulfate at 600 °C. The material prepared by gelation of chitosan beads in the presence of TiO$_2$ (CS/Ti/C-1) showed a rough surface (Figure 3c) consisting essentially of carbon with some agglomerates of TiO$_2$. The surface of the CS/TiS/C-1 material prepared with TiOSO$_4$ showed a low concentration of Ti, suggesting that the synthesis process led to the incorporation of Ti into the composite (Figure 3d).

TGA/DSC characterization of the composite microspheres before carbonization showed a thermal degradation profile like the crosslinked chitosan matrix (results not shown). Based on the residual mass after thermal treatment at 600 °C, TiO$_2$ percentages of
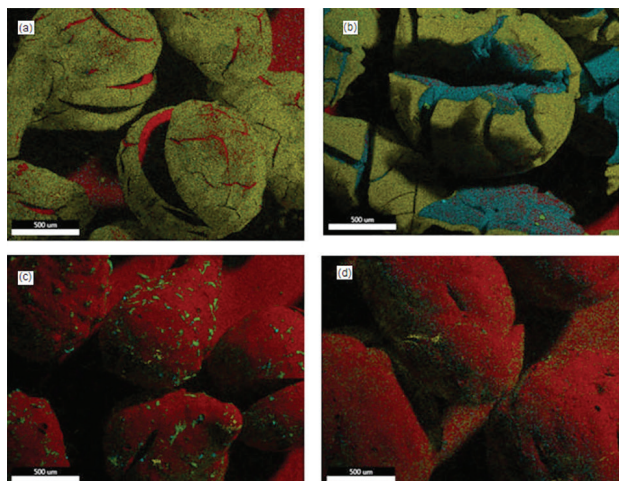
Figure 3. EDS distribution maps for the elements Ti (yellow), C (red), O (green), and S (blue): (a) CS/Ti/C-2; (b) CS/TiS/C-2; (c) CS/Ti/C-1; and (d) CS/TiS/C-1.

approximately 15% were estimated for CS/TiS/C-2 and CS/Ti/C-2, while values of around 5% were obtained for CS/Ti/C-1 and CS/TiS/C-1.

The FTIR spectra of the carbonized microspheres (Figure 4) were quite similar, with weak broad band centered at approximately 3400 cm^{-1}, corresponding to overlapping stretching vibrations of O–H and N–H, and weak bands at 2924 and 2849 cm^{-1}, assigned to aliphatic C–H stretching. A band at 1577 cm^{-1} was attributed to the stretching vibration of C=C bonds in the aromatic rings formed after carbonization.[35] Bands in the region 1260-1000 cm^{-1} were assigned to asymmetric stretching of C–O–C bridges or stretching of aromatic C–O.[36,37] Peaks at 785, 660, and 450 cm^{-1} in the spectra for the composites corresponded to Ti–O–Ti bonds, Ti–O bending, and Ti–O stretching.[38]

Nitrogen physisorption was used to determine the textural parameters of the different materials (Table 1). An important finding was that the microspheres synthesized
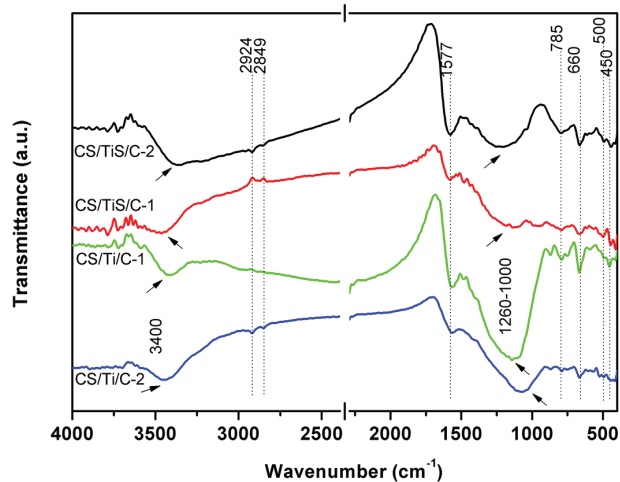

Figure 4. FTIR spectra (KBr pellets) of the composite microspheres.

using P-25 TiO₂ exhibited smaller surface area values (4.01 and 3.55 m^2 g^{-1} for CS/Ti/C-1 and CS/Ti/C-2, respectively), compared to those synthesized using TiOSO₄ (15.72 and 131.9 m^2 g^{-1} for CS/TiS/C-1 and CS/TiS/C-2, respectively). In addition, the surface area of CS/TiS/C-2 was greater than that of P-25 TiO₂. The pore size distributions showed that CS/TiS/C-1 possessed a microporous structure, while CS/Ti/C-1, CS/Ti/C-2, and CS/TiS/C-2 presented pore diameters of 2.01, 3.82, and 7.08 nm, which confirmed the presence of mesopores.

Table 1. Textural characteristics of CS/Ti/C-1, CS/Ti/C-2, CS/TiS/C-1, and CS/TiS/C-2

Material	Surface area / (m^2 g^{-1})	Pore size / nm	Pore volume / (cm^{-3} g^{-1})
CS/Ti/C-1	4.007	2.01	0.0041
CS/Ti/C-2	3.550	3.82	0.0060
CS/TiS/C-1	15.72	1.23	0.0097
CS/TiS/C-2	131.9	7.08	0.4621

CS/Ti/C-1: chitosan (CS) beads formed by dropwise addition of the CS solution to a solution of sodium hydroxide (2 mol L^{-1}) containing TiO₂ (2 g); CS/TiS/C-1: chitosan beads formed by dropwise addition of the CS solution to a solution of sodium hydroxide (2 mol L^{-1}) containing TiOSO₄ (2 g); CS/Ti/C-2: chitosan beads prepared and crosslinked, followed by leaving in contact with TiO₂ (0.4 g) in ethanol for 24 h; CS/TiS/C-2: chitosan beads prepared and crosslinked, followed by leaving in contact with TiOSO₄ (0.8 g) in isopropanol for 24 h.

These results showed that the incorporation of the titania precursors before carbonization caused changes in the initial textural characteristics of the carbon. During the calcination process in the range from 400 to 700 °C, occurs the decomposition of the TiOSO₄ outside the matrix and *in situ* generations of sulfate (SO₄$^{2-}$) ions that facilitates the synthesis of mesoporous and increase surface area, according to previous results in the literature.[39-41]

X-ray diffraction was used to characterize the phase compositions of the composite materials (Figure 5). The diffractogram for the Degussa P-25 TiO₂ showed all the peaks indexed for the anatase phase (JCPDS file No. 71-1167) and the rutile phase (JCPDS file No. 76-1939). All the microspheres showed amorphous halos (at 2θ of 20-30°), associated with the chitosan.[42] The CS/TiS/C-1 and CS/Ti/C-1 microspheres, with TiO₂ present within the composite, did not show the characteristic diffraction peaks of anatase or rutile TiO₂. Anatase was only evident in the case of the CS/Ti/C-2 composite (with TiO₂ present on the surface of the material), which presented a TiO₂ diffraction peak at 25.31° related to the anatase (101) crystallographic plane. In addition, there was no evidence of conversion from the anatase to the rutile structure on the TiO₂ composite materials used as photocatalysts.[43]
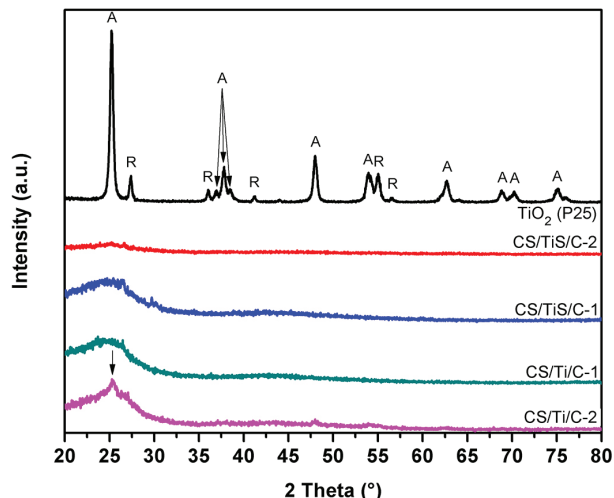
Figure 5. XRD patterns for Degussa P-25 TiO$_2$ (A = anatase; R = rutile); CS/TiS/C-2; CS/TiS/C-1; CS/Ti/C-1; and CS/Ti/C-2.

The Raman spectra of the CS/TiS/C-2 and CS/Ti/C-2 composite microspheres showed the presence of TiO$_2$ mainly in the form of the anatase phase (Figure 6), with five bands corresponding to the six active modes expected for anatase, according to group theory (A$_{1g}$ + 2B$_{1g}$ + 3E$_g$). These comprised a strong and sharp band at 154 cm^{-1} (E$_{g(1)}$ mode), a weak band at about 199 cm^{-1} (E$_{g(2)}$ mode), and three medium intensity bands at around 396 cm^{-1} (B$_{1g(1)}$ mode), 516 cm^{-1} (A$_{1g}$/B$_{1g(2)}$ modes), and 635 cm^{-1} (E$_{g(3)}$ mode). For both samples, the TiO$_2$ anatase phase was predominant, which was in agreement with the XRD data.[20,44-46]
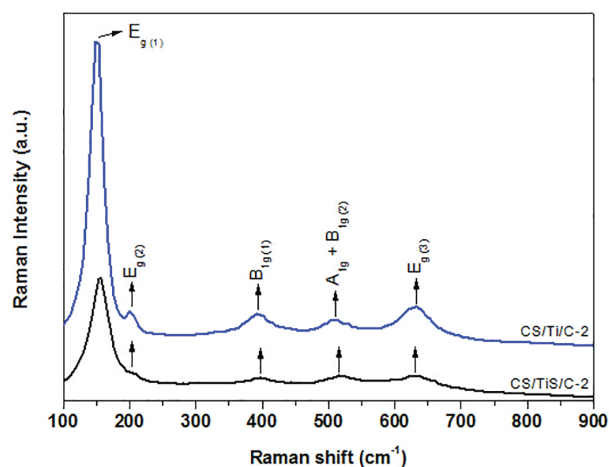

Figure 6. Raman spectra of the CS/TiS/C-2 and CS/Ti/C-2 composite microspheres.

It was not possible to observe the typical bands of TiO$_2$ in the Raman spectra for samples CS/TiS/C-1 and CS/Ti/C-1 because the titanium was immobilized within the chitosan microspheres during the preparation procedure. However, these samples showed two bands related to graphitized structures (Figure 7), the first at around

1349 cm^{-1}, corresponding to the D-band (commonly known as the defect or disorder band), and another at around 1579 cm^{-1}, corresponding to the G-band (known as the graphite band). The D-band indicates the presence of sp^3 defects in the graphite structure, while the G-band is related to all sp^2 carbon forms and provides information about the in-plane stretching vibration of sp^2 C−C bonds, which confirms the graphene-like structure composite materials. The G peak is proportional to the degree of disorder (D band).[46-48]
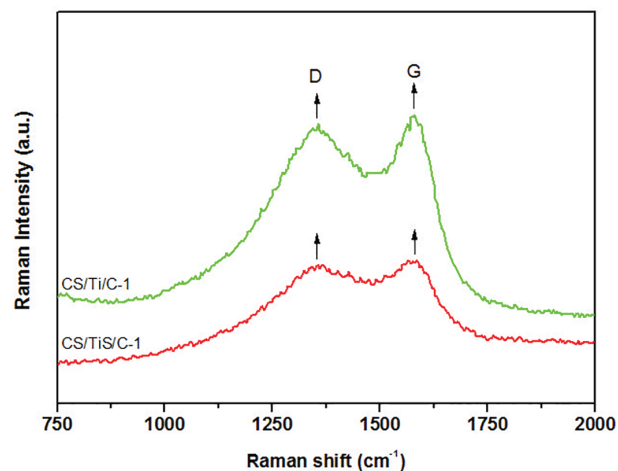

Figure 7. Raman spectra of the CS/TiS/C-1 and CS/Ti/C-1 composite microspheres.

The results of the XPS analysis provided valuable insights regarding the surface structures of the composite microsphere photocatalysts. Figures 8 and 9 show the Ti 2p and O 1s spectra for the CS/TiS/C-1 and CS/TiS/C-2 microspheres, respectively. The survey spectra for CS/Ti/C-1 and CS/Ti/C-2 exhibited two intense peaks for carbon and oxygen, which suppressed the Ti signal. The results for each element were evaluated, correlating the surface chemistry with the photocatalytic performance of the microspheres.[49]
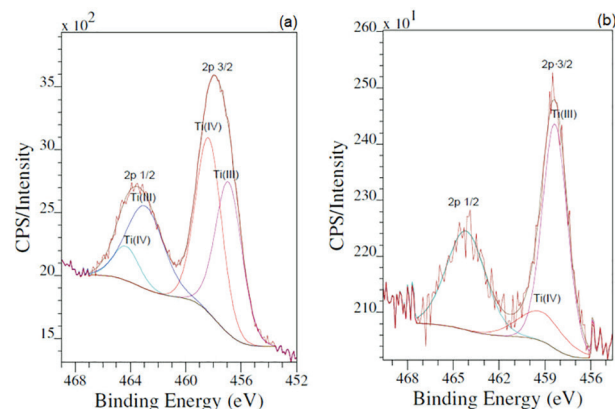

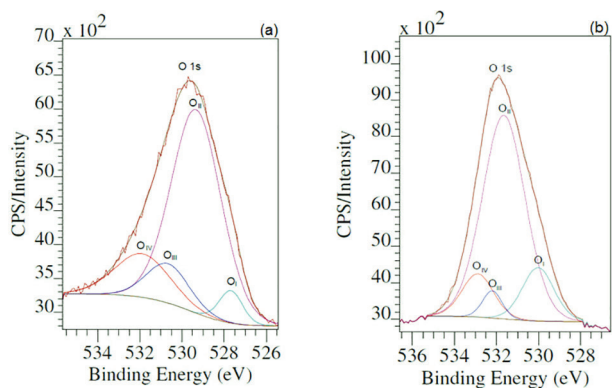**Figure 8.** Ti 2p XPS spectra for (a) CS/TiS/C-2 and (b) CS/TiS/C-1.

Figure 9. O 1s XPS spectra for (a) CS/TiS/C-2 and (b) CS/TiS/C-1.

The anatase TiO_2 (101) surface typically presents binding energies of 458.8 and 464 eV, corresponding to the 2p 3/2 and 2p 1/2 oxidation states of Ti^{4+}, respectively. A TiO_2 2p 3/2 binding energy at 457.9 eV corresponds to Ti^{3+} in Ti_2O_3, by removal of oxygen from the surface.[48] A ΔE (energy difference) value of 5.54 eV for spin-orbit splitting between Ti 2p 3/2 and Ti 2p 1/2 of TiO_2 indicates that Ti is predominantly in the form of Ti^{4+}.[49,50]

The detailed XPS spectrum of CS/TiS/C-2 (Figure 8a) showed peaks at 465.5 and 458.2 eV, corresponding to Ti 2p 1/2 and Ti 2p 3/2 of Ti^{4+}, respectively. The gap between the Ti 2p 3/2 and Ti 2p 1/2 lines was 5.6 eV, suggesting the predominant presence of the Ti^{4+} oxidation state. In addition, peaks at 463 eV (Ti 2p 1/2) and 456.7 eV (Ti 2p 3/2), assigned to Ti^{3+}, clearly indicated the presence of oxygen vacancies generated by the removal of O^{2-} from the lattice.[50-52] The spectrum for CS/TiS/C-1 (Figure 8b) featured peaks at 464.1 and 459.2 eV, corresponding to Ti 2p 1/2 and Ti 2p 3/2 of Ti^{4+}, respectively. An additional peak at 458.3 eV suggested the incorporation of C in the local Ti−O bond structure.[53] The intrinsic structural defects generated by Ti promoted the charge separation of photogenerated electron-hole pairs.[54]

The survey spectra of the samples showed an S 2p couplet at around 169 eV, consistent with a contribution of pure SO_4^{2-} from $TiOSO_4$. Additional contributions of Ti−O−S or $TiO_2−SO_4$ to the network oxygen in these samples could explain the significant chemical shift outside the usual O 1s region between 532 and 533 eV.[55-57]

The existence of Ti^{3+} and vacancies was corroborated by the deconvoluted O 1s XPS spectra (Figure 9). The XPS spectra were resolved into four asymmetric oxygen atom components, which were fitted considering the crystal lattice oxygen species for CS/TiS/C-1 and CS/TiS/C-2. The O_I photoelectron peaks (at 530 and 527.6 eV, respectively, for the two materials) could be attributed to lattice oxygen, indicating the formation of oxygen vacancies in the lattice.[58] The main O_{II} peaks of the samples, observed at

binding energies of 531.6 and 529.3 eV, respectively, were characteristic of metallic oxides.[59] The binding energies of O_{III} (at 532.2 and 530.6 eV) and O_{IV} (at 532.9 and 531.8 eV) corresponded to adsorbed hydroxide and molecular water on the rutile TiO_2 (110) surface, respectively.[50,51] The intensities of these peaks were in good agreement with the Ti 2p XPS spectra of the samples.

The materials band gap was not possible to calculate due to the high absorptivity of black materials.

Photocatalytic activity

Initially, to evaluate the photocatalytic activity of the obtained materials, SMX was selected as a model compound. Also, SMX is classified as a relevant emerging pollutant, since it can be found in different aquatic environments around the world, which reinforces its incomplete removal in the wastewater treatment plants.[60,61] Moreover, SMX can be used as a representative of the sulfa drugs (varying five-membered heterocyclic substituents), a class of antibiotics widely used in human and veterinary medicine.[62] The occurrence of antibiotics and pharmaceuticals in environmental samples brings up the concern about chronic ingestion and the unknown effects in human health and in aquatic biota and, especially the antibiotics can trigger bacterial resistance.[4,63]

The photocatalytic activity of the graphene-like composite materials was evaluated by the photodegradation of SMX in aqueous solution under UV-A radiation (Figure 10). For comparison purposes, experiments were also carried out to evaluate the degradation of SMX by photolysis (without the presence of photocatalysts) and by UV-A photocatalysis over P-25 TiO_2.

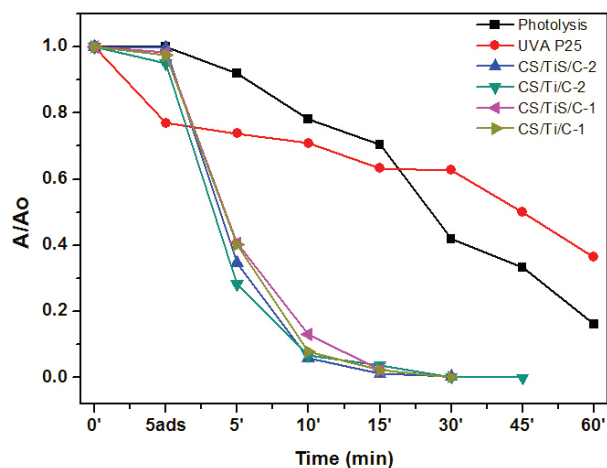Initially, the adsorption capacity of each synthesized materials was evaluated in the absence of irradiation,

Figure 10. Degradation of sulfamethoxazole (SMX) under UV-A irradiation (conditions: C_0 = 5 mg L^{-1} of SMX solution; pH 4 at 298 K).

with SMX removal lower than 5% in all cases. Based on this result, further experiments involved an adsorption-desorption equilibrium time of 5 min and subsequent irradiation for 60 min.

As related in the literature,[64] the SMX molecule is very photosensitive, which makes it easily degraded by UV-A photolysis. This behavior was observed, and the photolysis rate exceeded the degradation capacity of P25-mediate photocatalysis, as shown in Figure 10. Under photo-irradiation the SMX concentration decrease around 60% after 30 min, while 60% degradation was only achieved after 60 min in the presence of P-25 TiO_2. The low performance of P-25 TiO_2 could be explained by the fact that the powder was well dispersed in the suspension, which hindered the incidence of light on the active centers and consequently reduced the catalytic activity.[64,65]

In the presence of UV-A radiation, all synthesized materials showed higher photocatalytic activity than the reference photocatalyst (P-25 TiO_2), which allowed the almost complete removal of SMX in reaction times of 30 min (Figure 10).

It is universally accepted that the synergistic effect observed in the photocatalyst/activated carbon (AC) associations are due to the preliminary adsorption of substrates in the AC surface and its consequent approximation to the active sites on the photocatalyst surface.[66] This adsorption capacity is strongly influenced by the characteristic high porosity and specific surface area of typical AC, which permit the adsorption of greater quantities of organic reactants and fast diffusion of products during the photocatalytic reaction.[67,68] However, the carbon microspheres synthesized herein show a relatively low surface area (4.00 to 131.9 $m^2 g^{-1}$) and a low concentration of oxygenated functional groups (see Figure 4), resulting in low SMX adsorption rates (see Figure 10). Consequently, the increased rate constants observed with the application of irradiation could not be attributed to any synergistic effects associated with adsorption of the contaminants on the microspheres.

Materials synthesized by route 1 (CS/TiS/C-1 and CS/Ti/C-1) resemble a core-shell structure, with a shell consisting essentially of carbon. In materials of this type a sensitizing effect has been observed, in which exciting forms of carbon transfer electrons into the TiO_2 conduction band initiating the reaction.[69] Moreover, it is important to emphasize that the graphene-like carbonaceous matrix can contribute to the formation of persistent free radicals that lead to hydroxyl radical generation and that favor the degradation process, as observed in some studies involving the use of biochar.[70]

In materials synthesized by route 2 (CS/TiS/C-2 and CS/Ti/C-2) a homogeneous TiO_2 (anatase) distribution was observed on the surface of the carbonized cross-linked chitosan particles. In this type of composites, the presence of graphene-like structure facilitates the transport of photogenerated charges, which usually increases the photocatalytic activity.[71] The presence of carbon graphene-like materials allows the photogenerated electron to migrate fast from TiO_2 into the carbonaceous matrix, leading to the spatial separation of the electrons and holes. It thus enhances the lifetime of the charge carriers and therefore improves the efficiency of the photocatalytic process. The transferred electrons to carbon graphene-like materials diffuse befitting from the enhanced electrical mobility.[72,73]

It is well known that AC can influence the photocatalytic activities of different TiO_2 crystalline structures.[74,75] All the microspheres synthesized in the present work presented amorphous characteristics that could be attributed to the presence of interstitial carbons in the oxygen positions of the titanium dioxide lattice. These oxygen vacancies (Vo), related to the Ti^{3+} in the XPS spectrum, were responsible for rapid photo-induced charge separation and consequently to decreased electron-hole pair recombination in TiO_2. Consequently, a possible explanation for the high degradation efficiencies of the microspheres is a synergistic effect associated with the creation of defects and oxygen vacancies in the materials structures. The photocatalytic activities could be related to the effects of the Ti and O states on the Fermi energy, suggesting the existence of an ideal defects concentration for photocatalytic activity, above and below which the activity would decrease.[76] Based on the material structure, the mechanism proposed is due to the photogenerated electrons transferred from the valence band of TiO_2 to the Ti^{3+} and effective charge separation by carbon structure acts as an electron carrier due to the ballistic effect of π-conjugated aromatic rings (Figure 11).[76] These electrons are responsible for $^•O_2$ generated from O_2 molecules dissolved in the reaction solution and can be another active species for SMX degradation.

In order to explore material photocatalytic capacity, other compounds with a very different structure were
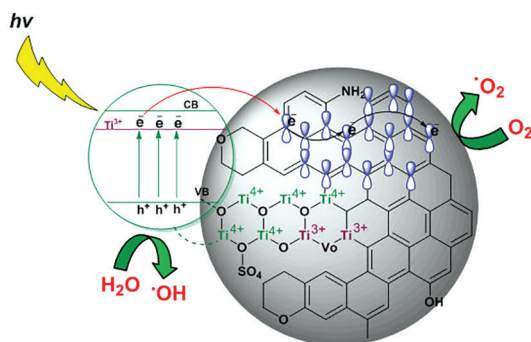

Figure 11. Proposed degradation mechanism of CS/TiS/C-2.

selected, CRP and HCT. These pharmaceuticals were selected since they are widely used in human medicine and, their occurrence in wastewater treatment plants were also reported in the literature.[60,77]

The degradation efficiency of CS/TiS/C-1 and CS/TiS/C-2 materials was also evaluated against aqueous solutions of CRP and HCT, and degradations of 98% in 30 min (Figure 12) for both contaminants were successfully obtained.
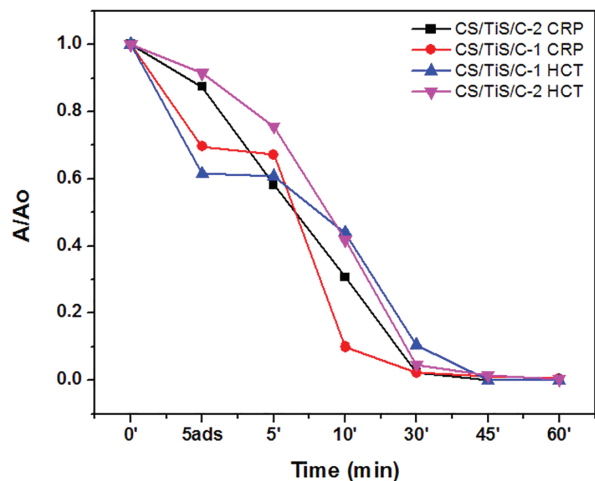

Figure 12. Photocatalytic degradation of chloramphenicol (CRP) and hydrochlorothiazide (HCT) under UV-A irradiation (conditions: $C_0 = 5$ mg L^{-1} CRP or HCT; pH 4 at 298 K).

It is important to reinforce the facility to remove the photocatalyst microspheres from the experiment solution, which allows collecting and reusing the photocatalysts. The catalyst reuse was evaluated in three consecutive cycles of SMX degradation. The study indicated the conservation of photocatalytic activity and preservation of the material structure, which suggests an excellent application potential.

Conclusions

Chitosan was successfully used as a precursor of carbonaceous materials employed as supports for TiO₂ photocatalysts. The experimental procedure was simple, reproducible, inexpensive, and enabled the synthesis of hybrid material with high photocatalytic activity. The degradation test results showed that adsorption of SMX on the materials was negligible and did not affect photodegradation performance. The immobilization of titanium on the spherical carbonized materials enhanced SMX, CRP, and HCT degradation, compared to the use of pure P-25 TiO₂. Data obtained from Raman, XPS, and XRD analyses revealed that the material had a graphene-like and amorphous structure, with oxygen vacancies that improved photocatalytic activity by separation of photogenerated

electron-hole pairs. In addition, the material could be reused at least 3 times, without any loss of photocatalytic efficiency.

Acknowledgments

References

1. Sousa, J. C. G.; Ribeiro, A. R.; Barbosa, M. O.; Pereira, M. F. R.; Silva, A. M. T.; *J. Hazard. Mater.* **2018**, *344*, 146.

2. Ebele, A. J.; Abdallah, M. A.; Harrad, S.; *Emerging Contam.* **2017**, *3*, 1.

3. Wee, S. Y.; Aris, A. Z.; *Environ. Int.* **2017**, *106*, 207.

4. Kümmerer, K.; *Chemosphere* **2009**, *75*, 417.

5. Midura-Nowaczek, K.; Markowska A.; *Perspect. Med. Chem.* **2014**, *6*, 73.

6. Yang, Y.; Ok, Y. S.; Kim, K. H.; Kwon, E. E.; Tsang, Y. F.; *Sci. Total Environ.* **2017**, *596-597*, 303.

7. Miklos, D. B.; Hartl, R.; Michel, P.; Linden, K. G.; Drewes, J. E.; *Water Res.* **2018**, *136*, 169.

8. Šrámková, M. V.; Diaz-Sosa, V.; Wanner, J.; *J. Water Process Eng.* **2018**, *22*, 41.

9. Kim, S.; Chu, K. H.; Al-Hamadani, Y. A. J.; Park, C. M.; Jang, M.; Kim, D. H.; Yu, M.; Heo, J.; Yoon, Y.; *Chem. Eng. J.* **2018**, *335*, 896.

10. Mir-Tutusaus, J. A.; Baccar, R.; Caminal, G.; Sarrà, M.; *Water Res.* **2018**, *138*, 137.

11. Klančar, A.; Trontelj, J.; Kristl, A.; Meglič, A.; Rozina, T.; Justin, M. Z.; Roškar, R.; *Ecol. Eng.* **2016**, *97*, 186.

12. Fujishima, A.; Zhang, X.; Tryk, D. A.; *Int. J. Hydrogen Energy* **2007**, *32*, 2664.

13. Gaya, U. I.; Abdullah, A. H.; *J. Photochem. Photobiol., C* **2008**, *9*, 1.

14. Shan, A. Y.; Ghazi, T. I. M.; Rashid, S. A.; *Appl. Catal., A* **2010**, *389*, 1.

15. Jonstrup, M.; Wärjerstam, M.; Murto, M.; Mattiasson, B.; *Water Sci. Technol.* **2010**, *62*, 525.

16. Duan, J.; He, X.; Zhang, L.; *Chem. Commun.* **2015**, *51*, 338.

17. Salaeh, S.; Perisic, D. J.; Biosic, M.; Kusic, H.; Babic, S.; Stangar, U. L.; Dionysiou, D. D.; Bozic, A. L.; *Chem. Eng. J.* **2016**, *304*, 289.

18. Bet-Moushoul, E.; Mansourpanah, Y.; Farhadi, K.; Tabatabaei, M.; *Chem. Eng. J.* **2016**, *283*, 29.

19. Khalid, N. R.; Majid, A.; Tahir, M. B.; Niaz, N. A.; Khalid, S.; *Ceram. Int.* **2017**, *43*, 14552.

20. Hayati, F.; Isari, A. A.; Anvaripour, B.; Fattahi, M.; Kakavandi, B.; *Chem. Eng. J.* **2020**, *381*, 122636.

21. Shahbazi, R.; Payan, A.; Fattahi, M.; *J. Photochem. Photobiol., A* **2018**, *364*, 564.

22. Leary, R.; Westwood, A.; *Carbon* **2011**, *49*, 741.

23. da Costa, E.; Zamora, P. P.; Zarbin, A. J. G.; *J. Colloid Interface Sci.* **2012**, *368*, 121.

24. Foo, K. Y.; Hameed, B. H.; *Adv. Colloid Interface Sci.* **2010**, *159*, 130.

25. Baek, M. H.; Jung, W. C.; Yoon, J. W.; Hong, J. S.; Lee, Y. S.; Suh, J. K.; *J. Ind. Eng. Chem.* **2013**, *19*, 469.

26. Shukla, S. K.; Mishra, A. K.; Arotiba, O. A.; Mamba, B. B.; *Int. J. Biol. Macromol.* **2013**, *59*, 46.

27. Olivera, S.; Muralidhara, H. B.; Venkatesh, K.; Guna, V. K.; Gopalakrishna, K.; Kumar K., Y.; *Carbohydr. Polym.* **2016**, *153*, 600.

28. Zawadzki, J.; Kaczmarek, H.; *Carbohydr. Polym.* **2010**, *80*, 394.

29. Hamden, Z.; Bouattour, S.; Ferraria, A. M.; Ferreira, D. P.; Ferreira, L. F. V.; do Rego, A. M. B.; Boufi, S.; *J. Photochem. Photobiol., A* **2016**, *321*, 211.

30. Zhu, H.; Jiang, R.; Xiao, L.; Liu, L.; Cao, C.; Zeng, G.; *Appl. Surf. Sci.* **2013**, *273*, 661.

31. Patze, S.; Huebner, U.; Liebold, F.; Weber, K.; Cialla-May, D.; Popp, J.; *Anal. Chim. Acta* **2017**, *949*, 1.

32. da Cruz, L. H.; Henning, F. G.; dos Santos, A. B.; Peralta-Zamora, P.; *Quim. Nova* **2010**, *33*, 1270.

33. Rybarczyk, M. K.; Lieder, M.; Jablonska, M.; *RSC Adv.* **2015**, *5*, 44969.

34. Kaczmarek, H.; Zawadzki, J.; *Carbohydr. Res.* **2010**, *345*, 941.

35. Araújo, B. R.; Romão, L. P. C.; Doumer, M. E.; Mangrich, A. S.; *J. Environ. Manage.* **2017**, *190*, 122.

36. Li, B.; Zhang, Y.; Yang, Y.; Qiu, W.; Wang, X.; Liu, B.; Wang, Y.; Sun, G.; *Carbohydr. Polym.* **2016**, *152*, 825.

37. Essawy, A. A.; Sayyah, S. M.; El-Nggar, A. M.; *RSC Adv.* **2016**, *6*, 2279.

38. Zeitler, V. A.; Brown, C. A.; *J. Phys. Chem.* **1957**, *61*, 1174.

39. Cao, L.; Xie, D.; Qu, Y.; Jing, C.; *Rare Met.* **2011**, *30*, 217.

40. Leghari, S. A. K.; Sajjad, S.; Zhang, J.; *RSC Adv.* **2013**, *3*, 15354.

41. Yu, C.; Chu, H.; Wan, Y.; Zhao, D.; *J. Mater. Chem.* **2010**, *20*, 4705.

42. Pandey, S.; Tiwari, S.; *Carbohydr. Polym.* **2015**, *134*, 646.

43. Huang, Y.; Ho, W.; Lee, S.; Zhang, L.; Li, G.; Yu, J. C.; *Langmuir* **2008**, *24*, 3510.

44. Payan, A.; Fattahi, M.; Jorfi, S.; Roozbehani, B.; Payan, S.; *Appl. Surf. Sci.* **2018**, *434*, 336.

45. Popa, M.; Diamandescu, L.; Vasiliu, F.; Teodorescu, C. M.; Cosoveanu, V.; Baia, M.; Feder, M.; Baia, L.; Danciu, V.; *J. Mater. Sci.* **2009**, *44*, 358.

46. Tan, L.-L.; Ong, W.-J.; Chai, S.-P.; Mohamed, A. R.; *Nanoscale Res. Lett.* **2013**, *8*, DOI 10.1186/1556-276X-8-465.

47. Štengl, V.; Bakardjieva, S.; Grygar, T. M.; Bludská, J.; Kormunda, M.; *Chem. Cent. J.* **2013**, *7*, DOI 10.1186/1752-153X-7-41.

48. How, G. T. S.; Pandikumar, A.; Ming, H. N.; Ngee, L. H.; *Sci. Rep.* **2014**, *4*, DOI 10.1038/srep05044.

49. Moulder, J. F.; Stickle, W. F.; Sobol, P. E.; Bomben, K. D.; *Handbook of X-Ray Photoelectron Spectroscopy*, 1st ed.; PerkinElmer Corporation: Minnesota, 1992.

50. Jackman, M. J.; Thomas, A. G.; Muryn, C.; *J. Phys. Chem. C* **2015**, *119*, 13682.

51. Jun, J.; Dhayal, M.; Kim, B. H.; Woo, H. G.; *J. Nanosci. Nanotechnol.* **2008**, *8*, 5537.

52. Jiang, X.; Zhang, Y.; Jiang, J.; Rong, Y.; Wang, Y.; Wu, Y.; Pan, C.; *J. Phys. Chem. C* **2012**, *116*, 22619.

53. Kurian, S.; Seo, H.; Jeon, H.; *J. Phys. Chem. C* **2013**, *117*, 16811.

54. Li, K.; Huang, Z.; Zeng, X.; Huang, B.; Gao, S.; Lu, J.; *ACS Appl. Mater. Interfaces* **2017**, *9*, 11577.

55. Baraket, L.; Ghorbel, A.; Grange, P.; *Appl. Catal., B* **2007**, *72*, 37.

56. Zhang, L.; Koka, R. V.; *Mater. Chem. Phys.* **1998**, *57*, 23.

57. Wang, Y.; Jiang, D.; Zhang, S.; Ou, M.; Bian, G.; Zhong, Q.; *J. Alloys Compd.* **2017**, *691*, 1005.

58. Khan, M. M.; Ansari, S. A.; Pradhan, D.; Ansari, M. O.; Han, D. H.; Lee, J.; Cho, M. H.; *J. Mater. Chem. A* **2014**, *2*, 637.

59. Nguyen-Phan, T. D.; Luo, S.; Liu, Z.; Gamalski, A. D.; Tao, J.; Xu, W.; Stach, E. A.; Polyansky, D. E.; Senanayake, S. D.; Fujita, E.; Rodriguez, J. A.; *Chem. Mater.* **2015**, *27*, 6282.

60. Luo, Y.; Guo, W.; Ngo, H. H.; Nghiem, L. D.; Hai, F. I.; Zhang, J.; Liang, S.; Wang, X. C.; *Sci. Total Environ.* **2014**, *473-474*, 619.

61. Benotti, M. J.; Trenholm, R. A.; Vanderford, B. J.; Holady, J. C.; Stanford, B. D.; Snyder, S. A.; *Environ. Sci. Technol.* **2009**, *43*, 597.

62. Boreen, A. L.; Arnold, W. A.; McNeill, K.; *Environ. Sci. Technol.* **2004**, *38*, 3933.

63. Kraemer, S. A.; Ramachandran, A.; Perron, G. G.; *Microorganisms* **2019**, *7*, 180.

64. Długosz, M.; Zmudzki, P.; Kwiecień, A.; Szczubiałka, K.; Krzek, J.; Nowakowska, M.; *J. Hazard. Mater.* **2015**, *298*, 146.

65. Dong, H.; Zeng, G.; Tang, L.; Fan, C.; Zhang, C.; He, X.; He, Y.; *Water Res.* **2015**, *79*, 128.

66. Xue, G.; Liu, H.; Chen, Q.; Hills, C.; Tyrer, M.; Innocent, F.; *J. Hazard. Mater.* **2011**, *186*, 765.

67. Yin, B.; Wang, J. T.; Xu, W.; Long, D. H.; Qiao, W. M.; Ling, L. C.; *New Carbon Mater.* **2013**, *28*, 47.

68. Saucier, C.; Adebayo, M. A.; Lima, E. C.; Cataluña, R.; Thue, P. S.; Prola, L. D. T.; Puchana-Rosero, M. J.; Machado, F. M.; Pavan, F. A.; Dotto, G. L.; *J. Hazard. Mater.* **2015**, *289*, 18.

69. Martins, A. C.; Cazetta, A. L.; Pezoti, O.; Souza, J. R. B.; Zhang, T.; Pilau, E. J.; Asefa, T.; Almeida, V. C.; *Ceram. Int.* **2017**, *43*, 4411.

70. Zhong, J.; Chen, F.; Zhang, J.; *J. Phys. Chem. C* **2010**, *114*, 933.

71. Fang, G.; Liu, C.; Wang, Y.; Dionysiou, D. D.; Zhou, D.; *Appl. Catal., B* **2017**, *214*, 34.

72. Tu, W.; Zhou, Y.; Liu, Q.; Tian, Z.; Gao, J.; Chen, X.; Zhang, H.; Liu, J.; Zou, Z.; *Adv. Funct. Mater.* **2012**, *22*, 1215.

73. Kim, I. Y.; Lee, J. M.; Kim, T. W.; Kim, H. N.; Kim, H.-i.; Choi, W.; Hwang, S.-J.; *Small* **2012**, *8*, 1038.

74. Li, Y.; Li, X.; Li, J.; Yin, J.; *Water Res.* **2006**, *40*, 1119.

75. Shao, X.; Lu, W.; Zhang, R.; Pan, F.; *Sci. Rep.* **2013**, *3*, DOI 10.1038/srep03018.

76. Xing, M.; Li, X.; Zhang, J.; *Sci. Rep.* **2014**, *4*, DOI 10.1038/srep05493.

77. Deblonde, T.; Cossu-Leguille, C.; Hartemann, P.; *Int. J. Hyg. Environ. Health* **2011**, *214*, 442.